LA-UR- 98-2147

Approved for public release; distribution is unlimited.

Title: ENERGETIC NEUTRAL ATOM IMAGING WITH THE POLAR CEPPAD/IPS INSTRUMENT: INITIAL FORWARD MODELLING RESULTS

CONF-9707186--

Author(s): M. G. Henderson, NIS-2
G. D. Reeves, NIS-2
K. R. Moore, NIS-1
H. E. Spence, Boston University
A. M. Jorgenson, Boston University
J. F. Fennell, Aerospace Corp.
J. B. Blake, Aerospace Corp.
E. C. Roelof, Johns Hopkins Univ., APL

Submitted to: "Physics and Chemistry of the Earth"

Proceedings for the Paros ISTP Symposium

July 1997

Paros, GREECE

Los Alamos
NATIONAL LABORATORY

DISCLAIMER

Energetic Neutral Atom Imaging with the POLAR CEPPAD/IPS Instrument: Initial Forward Modeling Results

M. G. Henderson[1], G. D. Reeves[1,*], K. R. Moore[1], H. E. Spence[2], A. M. Jorgensen[2], J. F. Fennell[3], J. B. Blake[3], and E. C. Roelof[4]

[1]Los Alamos National Laboratory, Los Alamos, New Mexico
[*]Presently at Max Planck Institut für Aeronomie, Katlenburg-Lindau, Germany
[2]Center for Space Physics, Boston University, Boston, Massachusetts
[3]The Aerospace Corporation, Los Angeles, California
[4]Johns Hopkins University Applied Physics Laboratory, Laurel, Maryland

Camera-ready Copy for

Physics and Chemistry of the Earth

Manuscript-No. ?????

Offset requests to:
M. G. Henderson
NIS-2 Mail Stop D436
Los Alamos National Laboratory
Los Alamos, New Mexico 87545
USA

Journal: Physics and Chemistry of the Earth
MS No.: ?????
First author: Henderson

Energetic Neutral Atom Imaging with the POLAR CEPPAD/IPS Instrument: Initial Forward Modeling Results

M. G. Henderson[1], G. D. Reeves[1,*], K. R. Moore[1], H. E. Spence[2], A. M. Jorgensen[2], J. F. Fennell[3], J. B. Blake[3], and E. C. Roelof[4]

[1]Los Alamos National Laboratory, Los Alamos, New Mexico
*Presently at Max Planck Institut für Aeronomie, Katlenburg-Lindau, Germany
[2]Center for Space Physics, Boston University, Boston, Massachusetts
[3]The Aerospace Corporation, Los Angeles, California
[4]Johns Hopkins University Applied Physics Laboratory, Laurel, Maryland

Received ?? September 1997 – Accepted ?? ????????? 1997

Abstract. Although the primary function of the CEPPAD/IPS instrument on Polar is the measurement of energetic ions *in-situ*, it has also proven to be a very capable Energetic Neutral Atom (ENA) imager. Raw ENA images are currently being constructed on a routine basis with a temporal resolution of minutes during both active and quiet times. However, while analyses of these images by themselves provide much information on the spatial distribution and dynamics of the energetic ion population in the ring current, detailed modeling is required to extract the actual ion distributions. In this paper, we present the initial results of forward modeling an IPS ENA image obtained during a small geo-magnetic storm on June 9, 1997. The equatorial ion distribution inferred with this technique reproduces the expected large noon/midnight and dawn/dusk asymmetries. The limitations of the model are discussed and a number of modifications to the basic forward modeling technique are proposed which should significantly improve its performance in future studies.

1 Introduction

Energetic neutral atoms (ENAs) are produced by charge exchange collisions that occur between energetic ring current/radiation belt ions and the cold neutral atoms that make up the Earth's tenuous extended exosphere (the geocorona). Once created, ENAs travel away in straight line trajectories unaffected by the Earth's magnetic field and hence behave much like photons. Since charge exchange occurs continuously in the inner magnetosphere, the Earth's ring current "glows" in the "light" of energetic neutral atom radiation. Some of the energetic neutral atoms that are directed Earthward undergo additional charge exchange collisions in the dense low altitude atmosphere and contribute to the formation of the low altitude equatorial radiation belt (Hovestadt et al. (1972) and Moritz (1972)). But most ENAs emitted from the magnetosphere freely escape into space where they can be remotely detected by appropriately instrumented spacecraft.

The first suggestion that the escaping ENAs could be used to remotely sense the magnetospheric energetic ion population was made by Hovestadt and Scholer (1976), and the first ENA image of the Earth's ring current was produced by Roelof (1987) from ISEE-1 energetic particle measurements. Since this initial work, energetic neutral atom images have been constructed from data acquired with the Swedish Astrid micro-satellite (C:son Brandt et al. (1997), Barabash et al. (1997)) and the Polar spacecraft (Henderson et al., 1997). The first ENA composition measurements from the GEOTAIL spacecraft have also been reported recently by Lui et al. (1996) and an upper limit on the quiet time ENA flux has been determined by Wilken et al. (1997) using the GEOTAIL HEP-LD instrument.

Although the analysis of raw ENA images alone can provide much information on the spatial distribution and dynamics of the magnetospheric energetic ion population, it is important to recognize that such images do not map out the distribution of ions directly. In order to obtain that information, detailed modeling of the charge exchange process is necessary (e.g. Roelof (1987), Chase and Roelof (1995)). In this study, we present the results of initial attempts at extracting the (modeled) global ring current distribution from an ENA image acquired by the Imaging Proton Spectrometer on-board the Polar spacecraft, during a small ($D_{st} = -78nT$) geomagnetic storm that occurred on June 9, 1997.

2 Instrumentation

The Imaging Proton Spectrometer (IPS) is part of a suite of instruments which together make up the Com-

Correspondence to: M. G. Henderson

prehensive Energetic Particle and Pitch Angle Distribution (CEPPAD) experiment on the Polar spacecraft. The IPS measures ions with energies in the range 14-1500 keV in 16 energy channels over 9 separate polar-angle look directions simultaneously. The field of view (FOV) centers for the detectors are arranged to be at 10°, 30°, 50°, 70°, 90°, 110°, 130°, 150°, and 170° with respect to the spin axis and each detector has an instantaneous FOV of 20° × 11.25° (for a combined instantaneous FOV of 180° × 11.25°). A complete 3-dimensional coverage of the unit sphere is obtained once every 6-second spin period.

Two different energy channels are used in the present work: the integral energy channel which is sensitive to energies greater than 17.5 keV, and the 17.5-22.6 keV differential energy channel. For the integral energy channel, counts are accumulated into 16 sectors per spin for the 10° and 170° detectors and 32 sectors per spin for all other detectors. For the 17.5-22.6 keV differential energy channel, counts are accumulated into: 32 sectors per spin for the 70°, 90°, and 110° detectors, 8 sectors per spin for the 10° and 170° detectors, and 16 sectors per spin for the remaining detectors. Because the detectors rotate during each accumulation interval, the effective angular response in the azimuthal direction is wider than the 11.25° instantaneous FOV. Due to the attitude of the Polar spacecraft, the scan plane of the 90° detector always intersects the Earth. Thus, the detectors with the highest angular resolution (the 70°, 90°, and 110° detectors) always scan closest to the Earth every spin.

Although the primary function of the IPS instrument is the detection of energetic ions *in-situ*, it also counts energetic neutral atoms (ENAs). However, since the instrument does not discriminate between ions and neutrals, ENAs can only be reliably identified when the flux of charged particles is very low. Fortunately, due to its highly elliptical polar orbit, Polar spends much of its time in the polar caps where this condition is usually satisfied. A more serious problem which afflicts both the analysis of energetic ions and energetic neutral atoms is that the detectors are sensitive to light. As a result, the detector(s) looking directly toward the Earth (and the Sun) will be contaminated. The sectors affected in this manner are usually just ignored. For a more detailed description of the IPS instrument see Blake et al. (1995).

3 Observations

In Fig. 1, we present observations of ENAs which were detected by the Polar CEPPAD/IPS instrument during a small geo-magnetic storm that occurred on June 9, 1997 (the provisional D_{st} index reached a minimum of -78 nT at approximately 4-5 UT). Integral energy channel ($E > 17.5$ keV) sector versus time plots for the 50°-150° detectors are shown in Fig. 1a. The radial distance (R), L-shell value (L), magnetic local time (MLT) and magnetic latitude (MLAT) of the Polar spacecraft are indicated at the bottom of the plot, below the time axis. Since the orbital period of Polar is ≈18 hours, more than a single orbit is presented in this 24-hour plot format. The data are shown in counts per second with blue indicating a low count rate, red indicating the highest count rate, and grey indicating a count rate of less than ~ 3.2 counts/s. At the beginning of the day, Polar was situated near apogee in the northern polar cap on its way down toward a southern polar cap perigee pass. The evening-sector ring current ions were encountered at ~0420 UT, the southern polar cap at ~0635 UT, the pre-noon ring current/radiation belt ions at ~0700 UT, and the northern polar cap at ~1000 UT. Following this, Polar remained in the northern polar cap for several hours up until ~2140 UT at which time the evening sector ring current ions were encountered again as Polar made its way toward a second southern perigee pass.

The enhanced energetic neutral atom emissions from the ring current can be seen as the inclined horizontal fuzzy bands in Fig. 1a when the spacecraft is situated in the polar caps (the predominantly grey regions). In addition to the ENA emissions, the response of the IPS instrument to Earth and Sun light is also visible. The sun contamination can be seen in sectors 0 and 1 of the 130° detector and sectors 0-3 of the 150° detector, while the Earth contamination can be seen in the 70°, 90°, and 110° detectors as the sharp, bright lines embedded in the weaker diffuse ENA emissions. Very strong evidence that the diffuse emissions are indeed ENAs comes from the fact that 1) they are clustered only around the line-of-sight direction toward the Earth, and 2) the POLAR CAMMICE MICS instrument – which is designed to reject neutrals – did not detect them (data not shown). Thus, together the CEPPAD/IPS and CAMMICE/MICS data unambiguously show that these emissions must be due to neutral atoms coming from line-of-sight directions that pass near the Earth.

An angle-angle plot (polar angle vs. azimuth angle) constructed by integrating the 17.5–22.6 keV (19.9 keV midpoint energy) ENA counts over the time period 0409:33–0419:33 UT is shown in Fig. 1b. The counts have been corrected for background and all pixels which may have been contaminated by earthlight or sunlight have been blanked out. As shown on the color bar to the right of this figure, the maximum count rate (of the pixels that remain) is approximately 22 counts/s. An Earthward–looking projection, derived from this angle-angle plot, of the IPS ENA pixels is shown in Fig. 1c. The FOV of this projection is 125° so only pixels from the 30°–150° detectors can be seen. The location of the Polar spacecraft at 0414:33 UT (the center time for the integration period) was $(-1.48, 3.33, 3.86)$ R_E (in solar-magnetic coordinates).

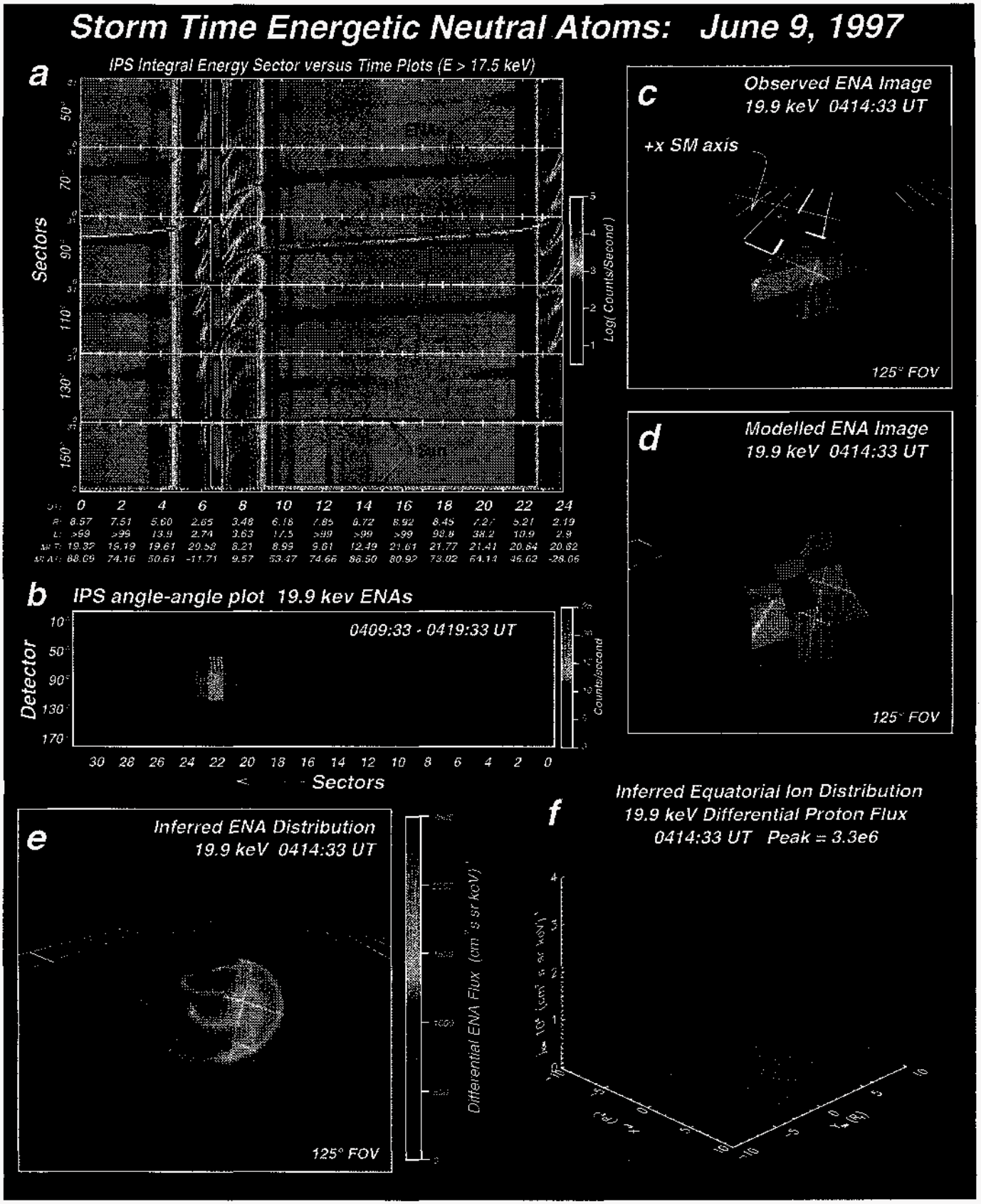

Fig. 1. Storm-time energetic neutral atom imaging on June 9, 1997. In (a), integral energy channel, sector vs. time plots for the 50°–150° detectors are shown. An (all-sky) angle-angle plot constructed from the 19.9 keV differential proton data is shown in (b), and (c) shows how the angle-angle plot pixels project onto the Earth as viewed from the vantage point of the IPS. The best-fit modeled ENA image is shown in (d), and the ENA distribution and equatorial ion distribution that was used to generate this modeled image are presented in (e) and (f).

4 Modeling ENAs

Except at very low altitudes where the exospheric neutral density is high, the inner magnetosphere is "optically thin" to the transport of energetic neutral atoms. Using this excellent approximation, the unidirectional differential flux of ENAs of a given species i, arriving at a given point in space $\vec{r}$, from a given direction $\hat{u}$, is given by;

$$j_{ena,i}(\vec{r},\hat{u},E) = \sigma_i(E)\int_0^\infty n_H(\vec{r}-s\hat{u})j_{ion,i}(\vec{r}-s\hat{u},\hat{u},E)ds \quad (1)$$

where σ_i is the energy dependent charge-exchange cross-section between the energetic ions and the cold exospheric neutral hydrogen atoms, n_H is the density of cold exospheric neutral hydrogen atoms, and $j_{ion,i}$ is the unidirectional differential flux of energetic ions of species i. The integration is taken along the line of sight (LOS) direction away from the detector $(-\hat{u})$ to ∞ (or to the surface of the Earth if $-\hat{u}$ intersects the Earth).

Although oxygen can be the dominant constituent of the ring current during large storms (e.g. Hamilton et al. (1988) and Daglis (1997)), H^+ is typically dominant for smaller storms like the one presented here (e.g. see Daglis (1997)). An empirical relationship relating the O^+/H^+ number density ratio (of 0.9-16 keV/e ions) near geosynchronous orbit to the K_p index and the adjusted solar 10.7 cm flux ($\bar{F}_{10.7}$) has been given by Young et al. (1982) as;

$$O^+/H^+ = 4.5\times10^{-2}\exp(0.17K_p + 0.010\bar{F}_{10.7}). \quad (2)$$

For the event presented here, $K_p = 6$ and $\bar{F}_{10.7} \approx 75$, giving $O^+/H^+ \approx 0.26$. Thus, to a crude first approximation, we may neglect all ion species except H^+ and derive an 'effective H^+ ring current'.

The cross section for H-H^+ charge exchange collisions is given by (Hodges, 1994);

$$\sigma = 2\times10^{-16}[5.82 - 0.929\log E]^2\mathrm{cm}^2 \quad (3)$$

where the ion energy E is in units of eV.

The exospheric neutral H density model we use is the spherically symmetric Chamberlain model (Chamberlain, 1963) with parameters as determined by Rairden et al. (1986). And the ion distribution we have adopted for this initial work is a 10-parameter model developed by Roelof et al. (1992), Roelof et al. (1993) and Chase and Roelof (1995). In this model, the ion distribution is specified in the equatorial plane as follows;

$$j_{ion} = j_\circ\exp(-F_\phi - F_L) \quad (4)$$

where F_ϕ and F_L are given by,

$$F_\phi = k_1[1-\cos(\phi-\phi_1)] + k_2[1-\cos\{2(\phi-\phi_2)\}]$$

$$F_L = \begin{cases} \frac{(L-L_1)^2}{2\delta L_1^2} & L < L_{11} \\ \frac{(L-L_{11})}{L_\circ} + \frac{1}{2}(\frac{\delta L_1}{L_\circ})^2 & L_{11} \le L \le L_{22} \\ \frac{(L-L_2)^2}{2\delta L_2^2} + \frac{(L_2-L_1)}{L_\circ} + \frac{1}{2}(\frac{\delta L_2}{L_\circ})^2 - \frac{1}{2}(\frac{\delta L_1}{L_\circ})^2 & L > L_{22} \end{cases}$$

and,

$$L_{11} = L_1 + \delta L_1^2/L_\circ$$

$$L_{22} = L_2 + \delta L_2^2/L_\circ$$

In this first attempt at forward modeling the POLAR CEPPAD/IPS ENA images, we follow the method of Roelof (1987) and take the ion distribution to be isotropic at the equator with an empty atmospheric loss cone. The distribution off of the equator is mapped adiabatically along dipole field lines according to Liouville's theorem.

5 Simulating POLAR ENA Images

The modeling described above allows one to construct theoretical ENA images with arbitrarily small angular resolution. These are extremely valuable in the interpretation of real (observational) ENA images. However, in order to compare observed and modeled images in a quantitative sense, the high-resolution theoretical images must be transformed to low-resolution images that the instrument would have observed. This process requires detailed knowledge of the instrumental angular response function. For the IPS instrument, each telescope has a rectangular aperture and a rectangular detector so that the instantaneous angular response is a "pyramid-like" function. As well, because the IPS is mounted on a spinning platform, this function gets smeared out in the azimuthal direction as shown in figure 2.

Once the angular response function is known, the ENA counts observed in a given sector by the IPS instrument can be computed as (e.g. Sullivan (1971), Roelof (1987));

$$C_{ij} = \Delta T\int_\theta\int_\phi\int_E A_{ij}(\theta,\phi)j_{ena}(\theta,\phi,E)\sin\theta d\theta d\phi dE \quad (5)$$

where $A_{ij}(\theta,\phi)$ is the angular response for a given sector, θ is the angle measured from the spin axis, and ϕ is the azimuth angle. Since ΔE is small for the differential channel used here, we can approximate the quantity $\int_E\sigma(E)j_{ion}(E)dE$ that results from combining 1 and 5 with $\bar{\sigma}j_{ion}$ where $\bar{\sigma} = \int_E\sigma(E)dE$ (which is approximately $34.44\times10^{-16}\mathrm{cm}^2\mathrm{keV}$ for the 17.5-22.6 keV channel).

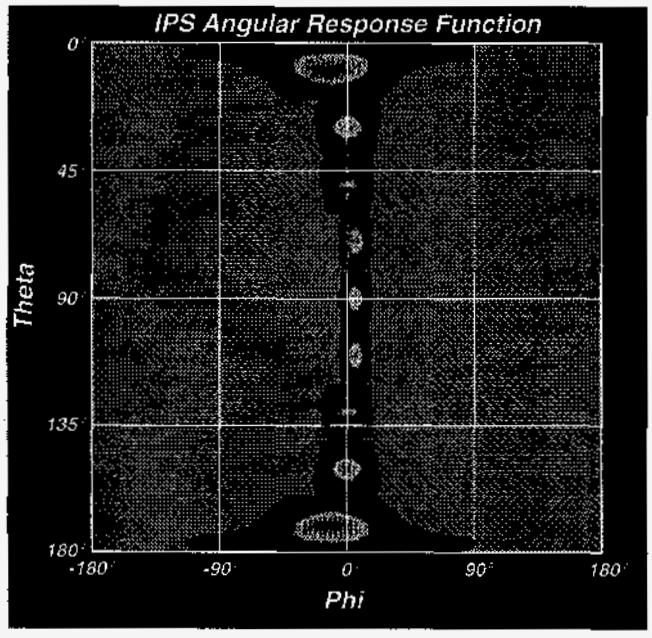

Fig. 2. Effective Angular response of the IPS instrument.

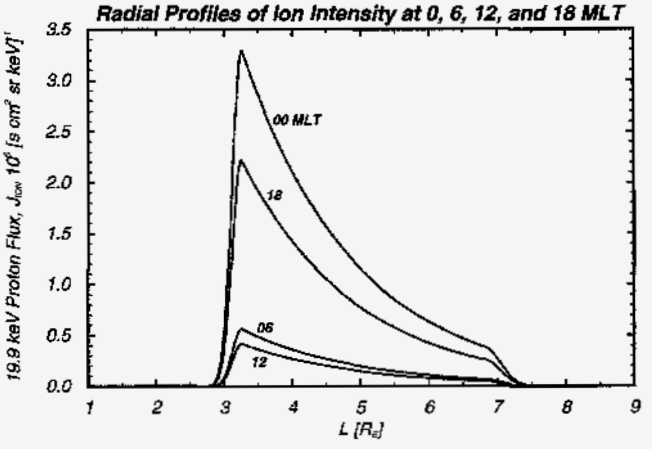

Fig. 3. Profiles of ion intensity at various magnetic local times inferred from energetic neutral atom emissions measured on June 9, 1997.

6 Fitting Data to Model

In order to minimize the difference between the measured and simulated Polar ENA images (in a least squares sense), we use Brent's variation on Powell's direction set method (see Brent (1973) and Lau (1995)). This line minimization technique is used because it does not require derivative information and is one of the most efficient algorithms of its class. However, a major drawback in using this method is that it does not guarantee that the global minimum will be found. Other methods like Simulated Annealing (SA) or Genetic Algorithms (GAs) (or hybrid approaches) are much more likely to return the global minimum, but are also enormously slow. This is a very serious limitation in modeling ENA images since it may take on the order of a few tens of seconds to simulate a complete ENA image. Parallelization of the code will allow us to implement these more sophisticated minimization techniques in future analyses.

7 Results

Figure 1d shows the modeled ENA image which best matches the observed IPS image. The inferred equatorial ion distribution is shown in figure 1f and a high resolution image of the ENA emissions resulting from the inferred model ring current is shown in figure 1e. It is important to note that (as discussed earlier) the brightest pixels near the Earth are ignored in the fitting process due to the fact that in the observed image they are contaminated by Earth light. In addition, the simple model used here is not valid at low altitudes below the exobase (where the medium is no longer 'optically' thin and the neutral composition is dominated by species other than hydrogen).

Nevertheless, as this first attempt at forward modeling a POLAR CEPPAD/IPS ENA image is intended only to demonstrate the dominant aspects of the global distribution of 19.9 keV protons at the D_{st} minimum (-78 nT) of a small geomagnetic storm, we feel that the limited model used here is sufficient. The pixel-by-pixel match between the observed 10-minute IPS image (Fig. 1c) and the simulation (Fig. 1d) is not perfect, due to the limitations of both the model and the minimization algorithm. However, a general trend can be seen in the images (Figs. 1c and 1d) for ENA emission to be brightest in the pre-midnight sector, implying both a noon-midnight and dawn-dusk asymmetry in the ring current. This trend is correctly manifested in the ion distribution that was fit to the data (Figs. 1e and 1f). It is detailed in the four MLT L-profiles of Fig. 2, where the inferred ion intensities are several times higher in magnitude at midnight (dusk) when compared to those at noon (dawn). The night-side dominance is consistent with the 33:1 midnight/noon ratio in the intensity of ring current ions of similar energies deduced from forward modeling an ENA image at the D_{st} minimum (-241 nT) of a considerably larger geomagnetic storm (Roelof, 1987).

In order to extract more detailed global ion distributions in future analyses, we need to adopt a more flexible ion model. A major limitation of the 10-parameter model of Eq. (3) is that j_{ion} is a separable function of L and ϕ. This means that the peak in the ring current must occur at the same L–shell value at all local times. Allowing F_L to depend on ϕ with the introduction of several more parameters will greatly enhance our ability to model the global ring current distribution more accurately.

In addition, more sophisticated minimization strategies need to be adopted – especially if the number of

model parameters increases beyond the 10 we already utilize. A major problem with simply minimizing the difference between the modeled and observed images in a least squared sense is that the model will tend to conform more closely to the brighter pixels. This is often not a desirable effect because a large portion of the information concerning the local time asymmetries and radial extent (and associated gradients) of the ring current is contained in the dimmer pixels. (Note that, in this respect, the removal of our light-contaminated pixels is not an altogether bad thing as these pixels would have been the brightest in terms of ENA emissions.) Several powerful techniques can be employed to help reduce these biases including: 1) the use of constraints on the modeled ENA images (e.g. force the model to be zero in locations where we know there are no counts), 2) the simultaneous minimization of multiple images taken from different look directions, and 3) the use of actual *in-situ* charged particle measurements from one or more spacecraft to constrain the ion model.

8 Conclusions

In this paper, we have presented our initial attempts at forward modeling the POLAR CEPPAD IPS energetic neutral atom images in order to infer the underlying equatorial ion distribution in the ring current during a small geomagnetic storm. The results obtained reproduce the expected gross features of the storm-time ring current ions in that they show large noon/midnight and dusk/dawn asymmetries with the peak intensity located in the pre-midnight sector. We have also discussed the limitations of the current work and proposed improvements to the forward modeling technique that will allow us to extract more information from the images in future analyses.

Acknowledgements. We gratefully acknowledge the following key scientists and engineers who contributed significantly to the IPS instrument: S. Imamoto, B. Johnson, W. A. Kolasinski, D. Mabry, J. Osborn, J. Skinner, F. Hilsenrath, C. Wilbur. This work was supported under NASA grant number S19511E. The efforts of E. C. Roelof at JHU/APL were partially supported by NASA Grants NAGW-2691 and NAGW-4729 to The Johns Hopkins University.

References

Barabash, S., C:son Brandt, P., Norberg, O., Lundin, R., Roelof, E. C., Chase, C. J., Mauk, B. H., and Koskinen, H., Energetic neutral atom imaging by the Astrid microsatellite, *Adv. Space Res., in press*, 1997.

Blake, J. B. et al., CEPPAD experiment on POLAR, *Space Sci. Rev.*, *71*, 531, 1995.

Brent, R. P., *Algorithms for Minimization without Derivatives*, Prentice-Hall, 1973.

Chamberlain, J. W., Planetary coronae and atmospheric evolution, *Planet. Space Sci.*, *11*, 901–960, 1963.

Chase, C. J. and Roelof, E. C., Extracting evolving structures from global magnetospheric images via model fitting and video visualization, *Johns Hopkins APL Technical Digest*, *16*, 111, 1995.

C:son Brandt, P., Barabash, S., , Norberg, O., Lundin, R., Roelof, E. C., Chase, C. J., Mauk, B. H., and Thomsen, M. F., ENA imaging from the Swedish microsatellite Astrid during the magnetic storm of 8 February, 1995, *Adv. Space Res., in press*, 1997.

Daglis, I. A., The role of magnetosphe-ionosphere coupling in magnetic storm dynamics, in *Magnetic Storms, Geophysical Monograph 98*, edited by V. T. Tsurutani, W. Gonzalez, Y. Kamide, and J. Arballo, pp. 107–116, AGU, Washington, D.C., 1997.

Hamilton, D. C., Gloeckler, G., Ipavich, F. M., Stüdemann, W., Wilken, B., and Kremser, G., Ring current development during the great geomagnetic storm of february 1986, *J. Geophys. Res.*, *93*, 14343–14355, 1988.

Henderson, M. G., Reeves, G. D., Spence, H. E., Sheldon, R. B., Jorgensen, A. M., Blake, J. B., and Fennell, J. F., First energetic neutral atom images from Polar, *Geophys. Res. Lett.*, *24*, 1167–1170, 1997.

Hodges, R. R., Monte Carlo simulation of the terrestrial hydrogen exosphere, *J. Geophys. Res.*, *99*, 23229, 1994.

Hovestadt, D. and Scholer, M., Radiation belt-produced energetic hydrogen in interplanetary space, *J. Geophys. Res.*, *81*, 5039, 1976.

Hovestadt, D., Häusler, B., and Scholer, M., Observations of energetic particles at very low altitudes near the geomagnetic equator, *Phys. Rev. Lett.*, *28*, 1340, 1972.

Lau, H. T., *A numerical library in C for scientists and engineers*, CRC Press, Boca Raton, 1995.

Lui, A. T. Y., Williams, D. J., Roelof, E. C., McEntire, R. W., and Mitchell, D. G., First composition measurements of energetic neutral atoms, *Geophys. Res. Lett.*, *23*, 2641, 1996.

Moritz, J., Energetic protons at low equatorial altitudes, *Z. Geophys.*, *38*, 701, 1972.

Rairden, R. L., Frank, L. A., and Craven, J. D., Geocoronal imaging with Dynamics Explorer, *J. Geophys. Res.*, *91*, 13613, 1986.

Roelof, E. C., Energetic neutral atom image of a storm-time ring current, *Geophys. Res. Lett.*, *14*, 652, 1987.

Roelof, E. C., Mauk, B. H., Meier, R. R., and Hulburt, E. O., Instrument requirements for imaging the magnetosphere in extreme-ultraviolet and energetic neutral atoms derived from computer-simulated images, *Proc. SPIE*, *1744*, 19, 1992.

Roelof, E. C., Mauk, B. H., Meier, R. R., Moore, K. R., and Wolf, R. A., Simulations of EUV and ENA magnetospheric images based on the Rice Convection Model, *Proc. SPIE*, *2008*, 202, 1993.

Sullivan, J. D., Geometrical factor and directional response of single and multi-element particle telescopes, *Nucl. Instr. and Meth.*, *95*, 5–11, 1971.

Wilken, B., Daglis, I. A., Milillo, A., Orsini, S., Doke, T., Livi, S., and Ullaland, S., Energetic neutral atoms in the outer magnetosphere: An upper limit obtained with the hep-ld spectrometer on board geotail, *Geophys. Res. Lett.*, *24*, 111, 1997.

Young, D. T., Balsiger, H., and Geiss, J., Correlations of magnetospheric ion composition with geomagnetic and solar activity, *J. Geophys. Res.*, *87*, 9077–9096, 1982.